Quantification of Methotrexate in Human Serum Using Surface-Enhanced Raman Scattering—Toward Therapeutic Drug Monitoring

Göksel, Yaman; Zor, Kinga; Rindzevicius, Tomas; Thorhauge Als-Nielsen, Bodil Elise; Schmiegelow, Kjeld; Boisen, Anja

Published in:
ACS Sensors

Link to article, DOI:
10.1021/acssensors.1c00643

Publication date:
2021

Document Version
Peer reviewed version

Quantification of Methotrexate in Human Serum Using Surface-enhanced Raman Scattering – Towards Therapeutic Drug Monitoring

Yaman Göksel[1]*, Kinga Zor[1 2], Tomas Rindzevicius[1 2], Bodil Elise Thorhauge Als-Nielsen[3], Kjeld Schmiegelow[3], Anja Boisen[1 2]

1 Center for Intelligent Drug Delivery and Sensing Using Microcontainers and Nanomechanics (IDUN), Department of Health Technology, Technical University of Denmark, Kgs. Lyngby, 2800, Denmark

2 BioInnovation Institute Foundation, Copenhagen N, 2200, Denmark

3 Department of Paediatrics and Adolescent Medicine, Rigshospitalet University Hospital, Copenhagen, 2100, Denmark

KEYWORDS: Surface-enhanced Raman scattering, Therapeutic drug monitoring, Quantitative SERS, Methotrexate, Point-of-care detection, Patient samples

ABSTRACT: Therapeutic drug monitoring (TDM) can improve clinical care when using drugs with pharmacokinetic variability and a narrow therapeutic window. Rapid, reliable and easy to use detection methods are required in order to decrease the time of analysis, and can enable TDM also in resource-limited settings or even at bedside. Monitoring methotrexate (MTX), an anti-cancer drug, is critical, since it is needed to follow the drug clearance rate and decide how to administer the rescue drug, leucovorin (LV), in order to avoid toxicity and even death. We show that with the optimized nanopillar assisted separation (NPAS) method using surface-enhanced Raman scattering (SERS) we were able to measure MTX in PBS and serum in the linear range of 5 to 150 μM and confirmed that MTX detection can be carried out even in the presence of LV. Additionally, when NPAS was combined with centrifugal filtration a quantification limit of 2.1 μM for MTX in human serum sample was achieved. The developed detection method enables fast detection (10 min) and quantification of MTX from human serum (>90% accuracy). Furthermore, we show the potential of the developed method for TDM, when quantifying MTX from clinical samples, collected from patients, who are undergoing high-dose MTX therapy.

Therapeutic drug monitoring (TDM) is defined as the quantification of drugs in biological fluids at defined time intervals, to follow the level of a drug concentration, with the goal to either maintain the concentration in blood in a therapeutic range or to ensure its clearance to avoid toxicity.[1,2] It is strongly suggested in various clinical settings to monitor drugs with a narrow therapeutic window and significant pharmacokinetic variance, in order to improve the efficacy of the treatment and to prevent adverse effects.[3] Thus, TDM contributes greatly to chemotherapy treatment procedures, since drugs administered in this field tend to show severe adverse effects that can lead to morbidity and mortality.[3,4]

Methotrexate (MTX), one of the drugs in the World Health Organization´s list of essential medicines, is an antifolate agent. Once administered, MTX interferes with the metabolism of folic acid, blocks protein production and cell proliferation.[5] It is one of the most widely used anticancer agents and utilized in the treatment of various tumors, such as lymphoma, osteosarcoma, breast cancer, and leukemia.[3,5] Though MTX can be administered in a wide range of doses (from 20 mg/m² to 33,000 mg/m²), most of the adverse effects occur at high-dose methotrexate (HD-MTX) regimen where the dose is above 500 mg/m².[6] Prolonged exposure to MTX can cause damage also in the healthy cells. Thus, when it is administered in high doses, the rescue drug leucovorin (LV) is also supplied to the patients in order to ensure that the level of MTX is kept below a toxic level for a prolonged period, to avoid toxicity.[4–6]

HD-MTX therapy is essential for acute lymphoblastic leukemia treatments of pediatric patients where the pharmacokinetic variance is significant.[7] According to several protocols, patients receive the dose intravenously for 24 hours.[8,9] Once the administration is completed, MTX concentration in blood is measured with timed intervals until the concentration falls below 0.2 μM.[8,9] To oversee this clearance period, TDM is required since the dosage of LV is adjusted according to the blood MTX concentration measurements.[5,6,10] The MTX blood concentrations above 250, 20, 10 and 1 μM, at 24, 36, 42 and 48 hours after the initial infusion indicates severely delayed MTX elimination. In the case of delayed MTX elimination, the effect of LV proved to be insufficient and to prevent adverse effects in such cases, carboxypeptidase G2 ($CDPG_2$) is adminis-

tered as an antidote.[9–11] But $CDPG_2$ is an expensive alternative to LV.[12] Thus, an assessment of its application also strictly relies on TDM.[11]

Quantification of MTX in clinics is carried out routinely by various standard analytical procedures and methods from blood samples.[13] High-performance liquid chromatography (HPLC) coupled with various detection methods such as UV-visible [14] and fluorescence [15] is proved to be an accurate method for quantification of MTX in biological samples. However, HPLC coupled with mass spectrometry (LC-MS) [16], is referred to as the benchmark method for TDM. These methods can quantify below the clinically required detection limits (0.2 μM) with high selectivity.[17,18] Nevertheless, these methods are not suitable for TDM in clinics due to the high cost of equipmentand the requirement of trained personnel. Thus TDM in clinical settings is mostly performed with automated, high throughput robotic systems performing immunoassays.[19,20] These assays are routinely used for MTX TDM purposes, even though they have a relatively lower specificity [21,22] and require costly reagents.

Employing one or more sample pretreatment processes such as protein precipitation [18,23], solid-phase extraction [24,25], liquid-liquid extraction [26,27] are proved to be critical for HPLC methods to reduce the complexity of the sample matrix. These sample pretreatment steps are the most time-consuming and labor-intensive stage of the analysis procedures. Conversely, immunoassays used for TDM require far less sample preparation.[21] The need for established laboratory settings for HPLC sample pretreatment and the costly automation systems of immunoassays prevent less resource-rich clinics to perform TDM. Moreover, the time needed for the analysis of samples, up to 4 hours in the case of immunoassays, leads to prolonged hospitalization time and potential delays in the administration of a rescue drug when applicable.

There are several sensors and detection methods in the research and development phase for TDM, which combine pretreatment methods with detection, developed for on-site monitoring [28] using optical [29], surface plasmon resonance [30,31] and electrochemical methods [32,33]. These methods can achieve clinically relevant detection of various drugs in biological samples with relatively inexpensive, portable equipment. TDM with Surface-enhanced Raman Scattering (SERS) has been reported as well.[34] One of the optical detection methods, with high potential for miniaturization [35,36] is Raman spectroscopy, a label-free technique that enables the detection of molecules using vibrational fingerprint spectra.[37,38] If required, molecule-specific spectra can further be processed by multivariate data analysis methods to eliminate the effects of interfering compounds.[37,38] However, spontaneous Raman scattering is a very weak effect, i.e. only a small amount of excitation light is scattered with the molecule-specific information (i.e. Raman scattered light).[38] In SERS, the Raman scattering signal can be tremendously enhanced using nanostructured plasmonic materials, which yields higher sensitivity.[39] The SERS enhancement in most well-designed plasmonic nanostructures can reach the magnitude of 10^8.[40]

Due to their sensitivity, selectivity and speed of analysis, SERS-based sensors have been used in various applications [41], such as food safety [42–44], biochemisty [45,46], forensics [47] and also TDM [34]. Although SERS substrates perform remarkably when detecting drugs in artificial matrices [48,49], once these drugs are analyzed in bodily fluids [50–52], detection performance significantly decreases due to the complexity of biological sample matrices. Thus, SERS is no exception and requires sample pretreatment and/or purification just like most of the other analytical methods.[34,43,44,46,53]

It was demonstrated that different SERS-based detection methods could be employed for performing TDM on a wide range of drugs such as imatinib, 6-mercaptopurine, 5-fluorouracil, and also MTX.[34] Jiang et al. were able to detected MTX in methanol down to 0.1 fM using modified Ag substrates.[54] Hidi et al. showed that SERS can be used to detect 0.17 μM of MTX in aqueous solutions.[55] Quantification of drugs in biological samples, such as blood and serum matrix proved to be possible when using nanoparticle embedded filter paper used for both filtration and detection in human serum samples by Fornasaro et al.[51] Relatively complex SERS spectra were analyzed by multivariate analysis techniques in order to overcome complexities caused by the biological sample matrix. Also, Chen et al. showed that it is possible to detect 1 nM in diluted serum using microsphere modified capillaries.[56] Recently, Parachalil et al. showed the possibility of using a robust size-exclusion filtration technique called centrifugal filtration to process human serum samples for MTX detection in human serum with Raman spectroscopy.[57] Additionally, Markina et al. were able to detect MTX in spiked human urine using SERS-active sorbent for solid phase extraction.[58] Furthermore, Subaihi et al. demonstrated that by combining HPLC with SERS-based sensing, it is possible to detect MTX and its metabolite in patient urine samples.[59] Even when combining detection with simple sample preparation, MTX detection with Raman spectroscopy or SERS is challenging, especially when aiming to reach the 0.2 μM detection limit in biological matrices. Recently, we have used gold-coated nano-pillar (NP) substrates as a filtration device.[42,60] Dense forest of NP structures creates capillary forces due to the narrow gaps between each other causing the liquid to spread across the substrate surface. During this liquid flow, bigger molecules are obstructed by NP's while relatively smaller molecules continue to move towards the dry areas of the substrate.[42]

In this work, we present for the first time, the detection of MTX from patient serum samples with SERS using minimal sample preparation. Silver-coated NP (AgNP) SERS substrates [61] are simultaneously used as a sample pretreatment and detection platform.[42,60] We optimize the separation of the target analyte from the sample matrix on the SERS substrate and propose a combination of centrifugal filtration step with the NP-assisted separation (NPAS) to further improve the sample pretreatment.

Materials and Methods

Chemicals and Sample Preparation

MTX (98% purity) was initially dissolved in 50 µL 1 M NaOH, and 2 mM stock solution was prepared in phosphate buffered saline (PBS), pH 7.4, which was aliquoted and stored at -20 ºC until further use. LV calcium (98% purity) stock solutions were prepared in PBS (pH 7.4) and freshly used. The MTX and LV stock solutions were used to freshly prepare standards in PBS, commercially available human serum (from human male AB plasma) and in serum of the patients undergoing HD-MTX treatment at Rigshospitalet, Copenhagen, Denmark).

The MTX standard solutions in PBS and human serum were mixed with methanol (MeOH) in various ratios of 1/1, 1/5 and 1/9 during the optimization. All aqueous solutions were prepared using ultrapure water (18.2 mΩ) from a Milli-Q purification system (Millipore Corporation, Billerica, MA, USA). Solvents, chemicals and samples were of analytical grade and purchased from Sigma-Aldrich (St. Louis, MO, USA) if not otherwise specified.

Fabrication of the AgNP SERS Substrates

The AgNP SERS substrates were fabricated using a two-step process: (i) the Si material reactive ion etching (RIE) and (ii) the silver metal deposition are described in detail elsewhere.[61] In short, polished 4-inch silicon wafers were etched using an RIE process in an SF_6/O_2 gas mixture for 4 minutes, which yields vertically standing SiNP structures (~400 nm in height, ~50 nm in width, the SiNP density is ~20 NP/µm²). To clean the SiNP surface, the structures were exposed to an O_2 plasma for 1 min (MESC Multiplex ICP, STS, Morgan Hill, CA, USA). In a second step, the SiNPs were coated by a 225 nm thick silver metal film, which yields mushroom-like structures with silver caps on top of the Si pillars. The Ag metal was deposited using a thermal evaporator (NANO36, The Kurt J. Lesker Company, PA, USA). Scanning electron microscopy (SEM) images of the fabricated AgNP SERS substrates were collected using Zeiss Supra VP 40 (Jena, Germany). Finally, the Si wafers containing AgNP structures were diced using a laser micromachining tool (D-09126, 3D-Micromac AG, Chemnitz, Germany) into 4 x 4 mm chips. To avoid AgNP surface damage, the wafers were diced from the backside and stored in a desiccator until further use.

NP-assisted Separation (NPAS) and SERS Detection

A fork-shaped holder (Figure 1a) was fabricated from transparent polyethylene terephthalate glycol-modified (PETG) (RS Components, Northants, UK) using a 3D printer (Prusa i3 MK2, Prusa Research, Prague, Czechia). Each holder was made to hold three SERS chips (Figure 1a), which were immobilized (Figure 1b), on the support with a double-sided pressure-sensitive adhesive (PSA, ARcare 90106, Adhesive Research, Limerick, Ireland) tape, cut into desired dimensions using precision blade cutter (CE-40, Graphtec Corp., Yokohama, Japan). The plastic 3D printed holder was fixed with adhesive tape to a micromanipulation unit (M-562, Newport, Irvine, CA, USA) to enable finite vertical movement in and out from the sample reservoirs (Figure 1a). Reservoirs were made by micro-milling (Mini-Mill/3, Minitech Machinery Corp, GA, USA) well shape structures in Teflon (Polytetrafluoroethylene) blocks (RS Components, Northants, UK). Each well was made to hold at least 50 µL liquid sample. As indicated in Figure 1c, the SERS chips were vertically descended into the reservoirs and immersed (~5%) into the 50 µL sample until the SERS chips got in contact with the liquid creating the immersion region. The immersed chips were kept in contact with the samples for 60 seconds, to allow the liquid to move through the dense NPs and to cover 100% of the chip surface.

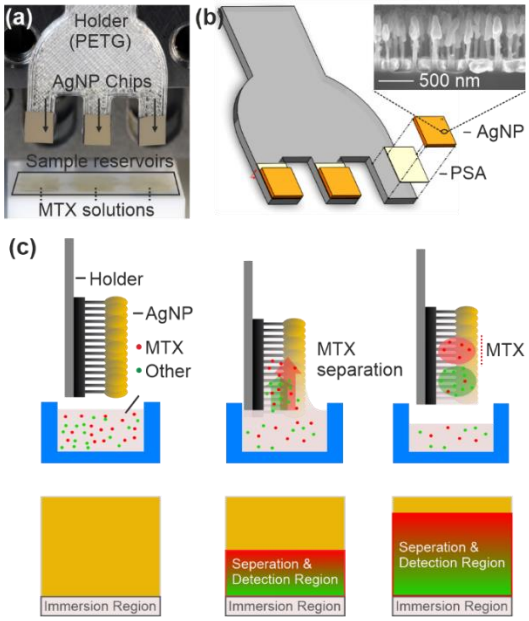

Figure 1. 3D printed sensor holder with the AgNP SERS chips attached to the immersion platform and positioned above the sample reservoirs (a). Schematic representation of the immobilization procedure of the SERS-chips to the sensor holder (b), SEM image of AgNPs from the side view, displaying NP forest (inset). Schematic representation of NPAS process, showing the movement of molecules on the SERS chip and the position of the immersion and separation/detection region at each step (c).

In this step, as the liquid moves through the separation/detection region, the small molecules (e.g. MTX) are gradually separated from larger components (e.g. proteins) present in the sample matrix. Next, the chips were removed from the reservoir and dried in a vertical position for 60 seconds (Figure 1c). During the drying process, the NP structures lean towards each other and cluster, creating "hot spots" where the Raman signal enhancement is most prominent [61]. Dried SERS chips were analyzed using a DXRxi Raman Microscope, (Thermo Scientific, Waltham, MA, USA) equipped with a 780 nm excitation laser, a 10x objective and a single grating spectrometer with 5 cm^{-1} FWHM spectral resolution and ± 2 wavenumber accuracy. The entire surface (4 x 4 mm) of the AgNP SERS chips were measured to create a map with 100 µm step size, resulting in at least 1600 spectra/map. All SERS measurements were performed with 10 mW laser power, 0.025 s point exposure time. Each point on the map was measured 5 times and acquired spectra were averaged.

Centrifugal Filtration of Serum Samples

As an additional sample preparation step, serum samples were filtered using an Amicon Ultra 0.5 mL centrifugal filter units (Millipore-Merck, Darmstadt, Germany), with a cutoff of 3 kDa. Before usage the filter units were pre-rinsed with MTX-free PBS solution. 300 µL human serum samples with varying concentrations of MTX were centrifuged at 10 600 g for 30 minutes (Centrifuge 5430, Eppendorf, Germany). The transparent filtrate material accumulated in the collection vials was gathered and analyzed afterward with the NPAS procedure as described above.

Data Analysis

The SERS data analysis was performed using an automated, custom-made Matlab (2018b, MathWorks, MA, USA) software package.[34] Each spectrum in the maps was background corrected by a linear model within the 660-700 cm^{-1} spectral range. The mean value for the 679 cm^{-1} MTX βC–C–C in aromatic ring vibration peak intensity was obtained from the top 20% of data for each SERS map, unless stated otherwise.[62,63] The limit of detection (LoD) was calculated based on 3σ/s where "σ" is the standard deviation of blank and "s" is the slope of the calibration curve. Similarly, limit of quantification (LoQ) was calculated based on 3.3 times of LoD. Data were plotted using Origin (2018b, OriginLab Corporation, MA, USA) and the calibration curves were constructed based on the measured averaged peak intensities. For data collection, at least three different SERS sensors were measured in an identical experimental condition.

Calculation of MTX Signal Coverage and MTX Separation on SERS Chips

ImageJ (http://rsb.info.nih.gov/ij/), freeware image software, was used to locate and calculate surface coverage of MTX signal (679 cm^{-1}) SERS map images. MTX signal presence changes the color of the SERS map from blue to red depending on the intensity of the MTX signal. Any location on the SERS maps with a color different than blue is located, and the surface coverage percentage is calculated by dividing this area by the area of the whole map. In order to measure the separation of the MTX from the immersed region, the "center of the mass" of located MTX signal was calculated. The distance of this center to the bottom of the SERS map measured in pixel units indicates the separation level of MTX from the sample matrix.

Quantification of MTX from Commercial Human Serum and Patient Serum Samples

For MTX quantification, commercially available human serum samples without and with centrifugal filtration were spiked with 68 and 12 µM MTX, respectively. Additionally, a three-point calibration curve was constructed in serum and in centrifugal filtered serum in a range from 15 to 100 µM and 2.5 µM to 15 µM, respectively. To demonstrate the clinical potential of the developed method, serum samples obtained from acute lymphocytic leukemia patients, treated with HD-MTX therapy, were analyzed with the NPAS procedure. Serum samples were obtained from 2 patients before (0 hour) and 24 hours after the initial MTX infusion. Calibration curves, based on three concentrations (25, 75, 125 µM MTX) were constructed in the control serum samples (0 hour), in order to assess the differences between patients. The obtained results were compared with competitive enzyme-linked immunoassay measurements done with identical samples using ARK Methotrexate Assay kits (Trexall, Arc Diagnostics, CA, USA) with Cobas 8000 modular analyzer (Roche Diagnostics, Rotkreuz, Switzerland). For commercial serum samples the accuracy of SERS-based quantification was calculated from the difference between predicted concentrations and known concentrations. Similarly, patient sample predictions were compared with the values obtained from immunoassay measurements.

Results & Discussion

Optimization of NPAS for PBS and Serum

Figure 2a, shows the regions observed after NPAS of commercially available serum samples spiked with MTX on the surface of SERS chips. In the photos as well as in the SEM images, it is visible that the majority of the macromolecules are present in the immersion region, while in the separation/detection region, there is much less or no macromolecules present. As it can be seen in Figure 2b and c the MTX signal intensity increases, as the molecule is further separated from the immersion region and from the serum sample matrix. The recorded MTX spectra in the separation/detection region display MTX characteristic features and are similar to the Raman spectra recorded from MTX powder (Figure S1). The benefit of using the NPAS method is clear, since as shown in Figure S2a,b with, commonly used drop-casting method for SERS-based sensing [61,64], a significant part of the SERS signal gets lost due to surface fouling of interfering molecules, i.e. proteins and salts as also previously shown by Morelli et al.[45]

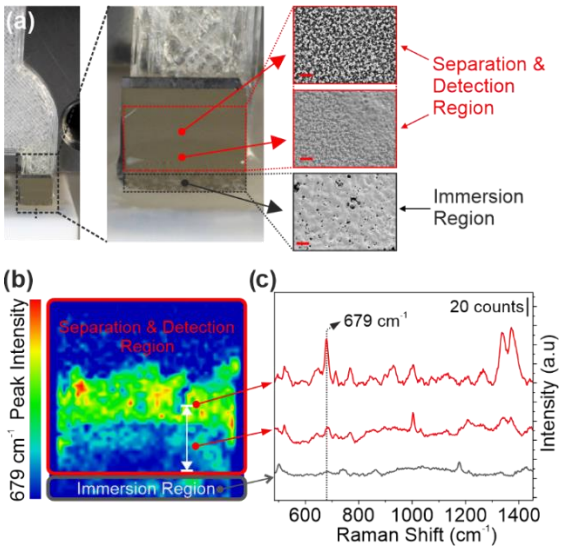

Figure 2. Photo of the NPAS setup (a, left), with defined regions observed after NPAS (a, middle) and SEM images obtained from corresponding regions (a, right). SERS map of

AgNP SERS chip after NPAS (10/50 serum/MeOH volume ratio at 50 µM MTX final concentration) where the color change of the map from blue to red indicates the 679 cm-1 signal intensity. The white arrow indicates the separation distance of MTX signal from immersion region (b). Representative SERS spectra of each indicated NPAS region on the SERS chips (c).

Due to the structure of the AgNPs, the SERS chips are intrinsically hydrophobic and require a wetting agent (e.g. organic solvents) to facilitate NPAS.[60] To enable the separation of MTX from the sample matrix MeOH was used as an organic solvent. When compared with other organic solvents (ethanol, DMSO) compatible with SERS-based detection of MTX, MeOH showed better performance in transporting the MTX molecules further away from the immersed region (data not shown). Additionally, MeOH caused precipitation of serum proteins (Figure S3) which further benefit the detection of MTX from serum, since the precipitated parts remain in the immersion region (Figure 2a).

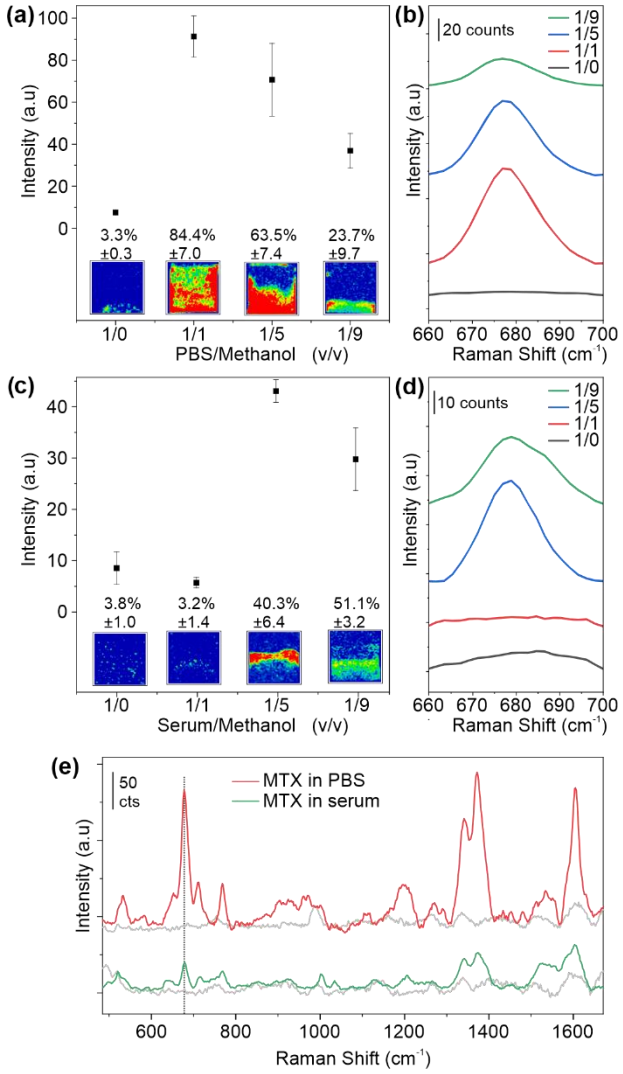

Figure 3. Intensity of SERS signal and surface coverage (insets) of 50 µM MTX in PBS (a) and serum (c) samples at different dilution ratios with MeOH. The insets (a,c) are representative maps for each dilution ratio, where the color change from blue to red indicates the 679 cm-1 signal intensity. Averaged SERS spectra for each SERS map obtained at the different dilution ratios in PBS (b) and serum (d). Averaged SERS spectra of samples (50 µM MTX) with optimal dilution ratios (1/1 for PBS (red line), 1/5 for serum (green line)) with indicating 679 cm-1 peak location, where the grey line is the signal recorded from control, PBS and serum without MTX (e). Error bars represent standard deviations between measurements, n=3.

In order to determine the optimal dilution proportion of sample to MeOH for NPAS, a series of dilution ratios (1/0, 1/1, 1/5 and 1/9) were evaluated. The SERS signal intensity of MTX in the separation/detection region as well as the separation distance of MTX from the immersion region were measured. We aimed to find the ratio, where the region of separated MTX is furthest from the immersion region and the MTX signal intensity is the highest. As the first step, we evaluated the effect of the separation using MTX spiked PBS samples. Even if PBS is a simple sample matrix, the presence of salt could obscure SERS-based detection.[45] As it is shown in Figure 3a and 3b, in the case of the MTX spiked in PBS samples, the highest MTX signal was obtained at 1/1 (PBS/MeOH, v/v) ratio, with MTX signal covering 84.4 ± 7 % of the sensor surface, with no detectable separation distance from the immersion region. Since the PBS matrix does not contain any macromolecule that can be separated using NP structures, the dilution of 1/1 ratio was considered optimum due to the intensity of the SERS signal and used for further measurements. In case of the commercial serum samples, the highest MTX signal recorded was obtained at the 1/5 ratio (serum/MeOH, v/v). As shown in Figures 3c and 3d, the surface coverage of the MTX signal was 40.3 ± 6.4%, with a visible separation of the MTX from the immersion region. At 1/5 dilution ratio, we observed the largest separation distance (134.4 pixels) compared to other dilution ratios (102.6 and 108.4 for 1/1 and 1/9 dilution ratios).

Figure 3e shows the difference in the MTX (50 µM) SERS spectral features, recorded in the separation/detection region after NPAS from PBS and serum samples with the optimal dilution. As expected, the MTX characteristic features appear well defined in PBS, due to the simplicity of the sample matrix. The MTX peak observed at 679 cm^{-1} (indicated with dashed lines) is attributed to βC–C–C in aromatic ring vibrations. This peak was utilized for quantification throughout the paper. Reportedly, other spectral features of the MTX molecule (768 cm^{-1}, 1371 cm^{-1} peaks assigned to γC–C–N and CH_3 vibrations respectively)[65] can also be used for identification of MTX, when using the Partial Least-Squares Regression model to quantify MTX in complex sample matrices i.e. patient samples, in the presence of other drugs. Although the SERS signal intensity is an important indicator, reproducibility and surface coverage are also crucial, especially when aiming for reproducible separation of the target analyte from the serum matrix. As shown in Figure 3a,c, the intensity of the recorded MTX signal is reproducible with 11.1 % and 5.2 % RSD for optimum PBS and serum cases, respectively.

Detection of MTX from PBS and Serum Assisted by NPAS and the Effect of LV Presence

SERS-based detection of various concentrations of MTX spiked in PBS and commercially available serum was carried out after the NPAS. Changes in the MTX characteristic 679 cm-1 signal intensity with varying concentrations of MTX is shown in Figure S4a and S4b for PBS and serum. As it can be seen in Figure 4a, the SERS signal intensity starts to saturate after 150 µM and loses its linear relation to MTX concentration, which could be due to a limited "hot spot" area around AgNP structures where the Raman signal is enhanced. There is a difference between the slope of the calibration curves obtained in PBS and serum, which could be due to the lower complexity of the PBS matrix.

As presented in Figure 4a, the calibration curves for both PBS and serum, have a linear correlation between MTX concentration and SERS signal intensity, from 5 to 150 µM (Figure 4a inset). The calculated LoD and LoQ values for PBS were found to be 6.3 µM and 20.9 µM,respectively. In the case of serum samples LoD and LoQ values are calculated as 8 µM and 26.5 µM, respectively. As reported by Skärby et al., observed average serum MTX concentration at 23 hours after administration of MTX was above 70 µM for patients from all risk groups. The obtained LoD and LoQ values and the data presented in Figure 4b indicate that dose adjustment with the rescue drug, LV, would be possible with NPAS method.[66]

SERS-based MTX detection in different sample matrices has been described in the literature. Hidi et al. reported the detection of MTX in PBS with a clinically relevant LoD of 0.17 µM using silver nanoparticles in a microfluidic system.[55] Fornasaro et al. were able to detect 1.08 µM MTX in an artificial matrix (4% BSA, PBS) and 31.57 µM in diluted human serum samples by applying Partial Least-Squares Regression model.[51] Parachalil et al. were able to detect 7.8 ± 5 µM in human serum after applying centrifugal filtration pretreatment to serum samples.[57] Without any further sample pretreatment than the 'build-in' NPAS, our proposed method appears to be comparable with these more elaborate sensing approaches.

Due to its similarity to MTX (Figure S5a inset) it is important to investigate if LV interferes with MTX detection. LV is essential in the HD-MTX treatment procedure, since in order to prevent the toxic effects of MTX, equimolar LV is administered to patients during the clearance stage of the therapy.[67] The structural similarities of these molecules can be observed in the powder Raman spectra (Figure S5a). Additionally, drop-casted 2 mM (5 µL) samples from each drug on SERS chips resulted in similar spectral features (Figure S5b). The signal originated from βC–C–C vibrations in aromatic ring structure is present in both molecules observed at 679 cm^{-1} for MTX and at 686 cm^{-1} for LV. Yet, SERS signals recorded from each molecule yield different intensities, with the βC–C–C vibrations signal in MTX recorded with 5 folds higher intensity compared to LV. As shown in Figure 4b, there was no contribution from LV when detecting MTX, since the calibration curve in the absence and in presence of LV was comparable. In order to observe LV signal (679 cm-1) with the NPAS method, we increased the concentration until 500 µM (Figure S5c,d). Moreover, when measuring MTX in the presence of LV from commercially available serum samples, we found that LV does not interfere with MTX detection (Figure S6a).

Effect of Centrifugal Filtration Combined with NPAS for the Detection of MTX from Serum

In order to evaluate if the LoQ can be further decreased, we used a centrifugal filtration pretreatment step, when working with human serum samples. As shown in Figure S7 molecules smaller than a 3kD cut-off value diffuse through the pores of the filter with an exerted centrifugal force, while larger molecules remain in the filter unit. We found that the NPAS procedure proved to be important also in the case of the pretreated commercially available serum samples, since there are compounds in the sample that interfere with the SERS-based detection (Figure S2c). The optimal sample/MeOH ratio for centrifugal filtered serum samples was found to be the same as for PBS samples (i.e. 1 to 1) (Figure S8a,b).

Once compared to the commercially available human serum samples that were processed with NPAS, the effect of the centrifugal filtration pretreatment step on MTX detection can be seen in Figure 5a. After centrifugal filtration, the MTX signal from 679 cm^{-1} was shifted to 687 cm^{-1}, thus

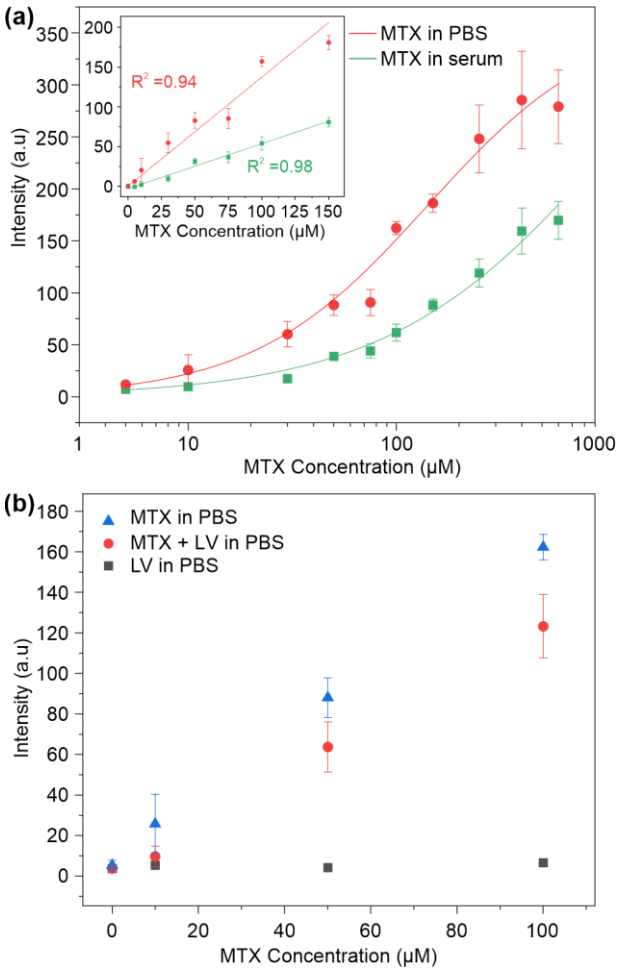

Figure 4. Calibration curves of MTX in PBS and serum, showing the relation between the intensity of the 679 cm-1 peak and MTX concentration. The linear part of the calibration curve is shown in the inset with R2 values for each linear fitting (a). Calibration curves of LV, MTX and equimolar MTX

LV mixtures in PBS recorded after NPAS, constructed using the intensity of the 679 cm-1 (b). All spectra shown are average of 3 measurements and error bars indicate standard deviation, n=3.

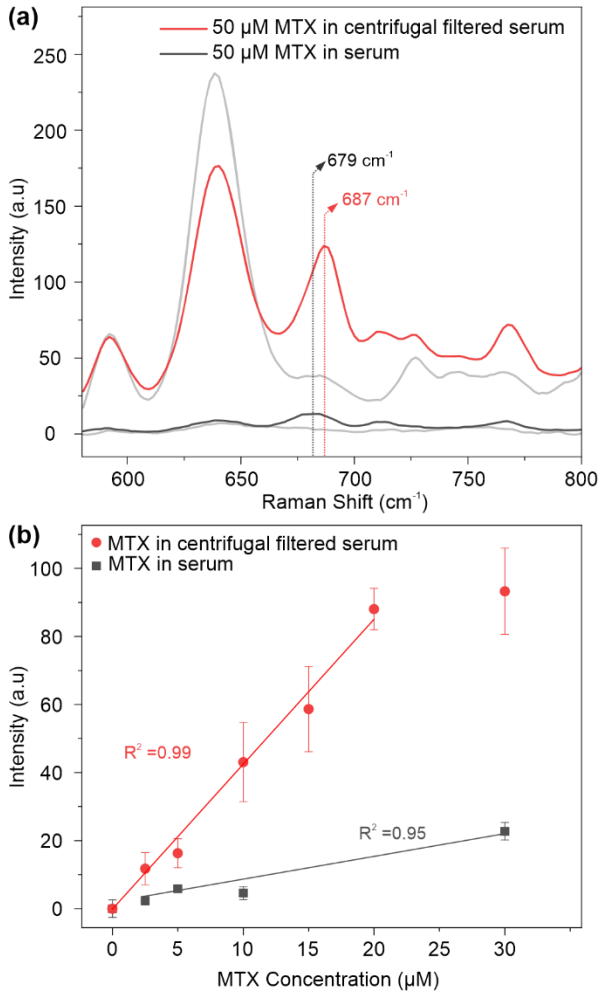

Figure 5. ~~Schematic representation of the centrifugal filtration process of serum samples (a).~~ Averaged SERS spectra of 50 µM MTX in serum samples after centrifugal filtration and NPAS (red line) and NPAS alone (black line), with the grey line representing the spectra of control (0 µM MTX) for each corresponding method. Dashed lines indicate the MTX peak location for each method (a~~b~~). Calibration curves with linear fittings of MTX in serum samples after centrifugal filtration and NPAS (red) and NPAS alone (black) with 687 cm-1 and 679 cm-1 peak positions respectively (b~~e~~). Error bars indicate standard deviation, n=3.

the applied baseline correction also shifted from 660-700 cm-1 to 664-704 cm-1 range for centrifugal filtered samples. As it can be seen in Figure 5a (grey and red line) additional strong peaks appear in the pretreated sample spectra. We also noticed that centrifugal filtration leads to an increased MTX signal intensity. The peak at 637 cm^{-1}, also present in the control, indicates the presence of other small molecules (e.g. uric acid) [68] that passed through the filters and settled on top of the AgNP structures (Figure S8c). For comparing the linear range of centrifugal filtered samples with the NPAS approach alone we worked in a linear range up to 30 µM. Figure 5b, shows the calibration curves obtained with non-pretreated serum samples and samples, which underwent centrifugal filtration. It can be seen that there is a linear dependency between MTX concentration and SERS signal between 0 to 20 µM in pretreated serum samples, with LoD of 0,6 µM and LoQ of 2.1 µM. This is a 12 fold decrease compared to non-centrifuged samples. In the case of non-pretreated samples the liner range was between 0 and 150 µM (Figure 4a). The difference between the calibration curves obtained from serum, without centrifugal filtration presented in Figure 4a and Figure 5b~~e~~, is due to the used SERS substrates obtained from different fabrication batches, which is within the range of variations reported by Morelli et al. with similar NP SERS substrates.[45]

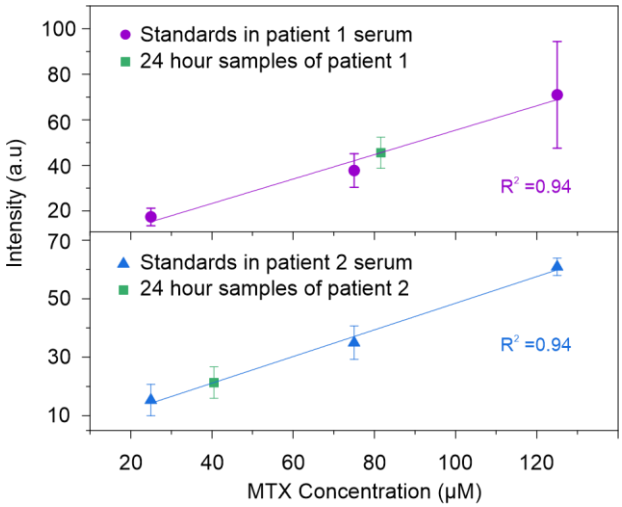

Figure 6. Quantification of MTX after NPAS in patient samples after 24 hours of initial MTX infusion for patient 1 (purple and green) and patient 2 (blue and green). Error bars indicate standard deviation, n=3.

In comparison with a previously reported SERS-based MTX detection approach, we found that the obtained LoD in commercial human serum with centrifugal filtered serum combined with NPAS is approximately 10 folds lower than the one reported by Parachalil et al. after similar centrifugal filtration.[57] Furthermore, the effect of the presence and absence of LV in MTX spiked centrifugal filtered serum samples is also shows that SERS intensity contribution of LV at 687 cm-1 was not observed at 100 µM, which is well above the linear range of MTX detection in centrifugal filtered serum samples (Figure S6b).

Quantification of MTX from Commercial Serum and Patient Serum Samples

In order to assess the applicability of the NPAS method used in combination with centrifugal filtration or without this pretreatment step, we quantified MTX from commercially available human serum spiked with 12 and 68 µM MTX, respectively. The calibration curves (Figure S9a,b) were used to quantify the amount of MTX from the spiked samples. We found that, when NPAS was used in combination with centrifugal filtration for the 12 µM sample, the

calculated concentration was 12 ± 2.3 μM. On the other hand, when NPAS was used without sample pretreatment, in the case of 68 μM containing samples, the calculated concentration was found to be 73.3 ± 7.7 μM. As shown in Figure S9c, the calibration curves obtained from patient samples are less sensitive, compared to the calibration curve obtained with commercial serum samples from healthy individuals. This difference is probably due to the complexity and differences between the patient serum samples. We also noticed that there is a difference in transparency and turbidity when comparing the patient samples. The quantification of MTX in patient samples was based on the standard curve obtained from the respective serum samples collected before MTX treatment at 0 h (Figure 6).

We found that MTX concentration at 24 h was 81.6 μM and 40.5 μM for patient 1 and patient 2, respectively. The MTX quantified with the NPAS approach proved to be comparable (85.4 μM and 64.3 μM) with the results from the analysis carried out at the hospital using a competitive enzyme-linked immunoassay. The underestimated MTX concentration for patient 2 could be due to the heterogeneity of the patient samples. Furthermore, MTX quantification after centrifugal filtration in 24 h samples of patient 2, yielded similar underestimation in quantification. The obtained data shows that NPAS has the potential for MTX monitoring in clinical settings. However, it is essential that additional patient samples are evaluated in future studies and that the quantification is carried out with more than 3 point calibration. Furthermore, there is a need for improving the sample pre-treatment step.

Conclusion

In this work, we present a rapid and practical method for TDM of MTX in human serum samples with SERS. With the optimized solvent sample ratio, the AgNP SERS chips proved to be suitable for separating the target analyte, MTX, from serum proteins. In NPAS, the MTX molecules pass through the compact NP structures, while the large molecules are accumulated at the immersion part of the sensor. The LoD for MTX in PBS (6.3 μM) and in human serum (8 μM) indicates the efficiency of the NPAS procedure combined with SERS-based detection. Additional centrifugal filtration step for serum samples further decreased the detection limit (0.7 μM).

To the best of our knowledge, the achieved LoD (0.6 μM) and LoQ (2.1 μM) in commercial human serum samples is the lowest in the so-far reported data with SERS-based MTX detection. Total analysis time for each sample is 10 minutes for NPAS, and 40 minutes once NPAS is combined with centrifugal filtration. With NPAS method, we were able to quantify commercial human serum samples with more than 90% accuracy with and without centrifugal filtration pretreatment step. Our proposed method showed no SERS signal interferences with rescue drug LV. Even though the entire clinical detection range (250 μM to 0.2 μM) is still not fully within reach, dose adjustment of the LV and identification of delayed MTX elimination is possible for a wide range of patients. MTX quantification from serum samples obtained from leukemia patients, undergoing HD-MTX show the potential of the NPAS-based method for TDM of MTX in clinical settings. 79% accuracy is achieved in quantifying patients samples, considering the MTX concentration found with the reference method, a competitive enzyme-linked immunoassay. For validation of the developed method, additional patient samples would need to be analyzed in the future.. Furthermore, there is a need for improving the sample pre-treatment step to achieve more accurate quantification. Moreover, the presented approach could be a suitable for miniaturization and automation by incorporating these simple sample pretreatment steps in a e.g. microfluidic system as shown before.[42,53,60]. Compared to established TDM methods, detection with NPAS combined SERS can be fast and instrumentation can be inexpensive and portable.

ASSOCIATED CONTENT

Supporting Information. This material is available free of charge via the Internet at http://pubs.acs.org."

Raman spectra of MTX powder and MTX spiked serum, NPAS drop-casting comparison, protein precipitation images, research on effect of leucovorin on MTX detection, schematic representation and optimization of centrifugal filtration of serum samples, calibration curves of quantification of MTX in serum and *95% confidence and prediction bands for calibration plots*.

AUTHOR INFORMATION

Corresponding Author

* Yaman Göksel - Center for Intelligent Drug Delivery and Sensing Using Microcontainers and Nanomechanics (IDUN), Department of Health Technology, Technical University of Denmark, Kgs. Lyngby, Denmark
Email: yagok@dtu.dk

Notes

The authors declare no competing financial interest.

ACKNOWLEDGMENT

YG acknowledges Elodie Dumont, Ph.D. for guidance and advice provided during the quantification of MTX from clinical samples and Lasse H. E. Thamdrup for SERS substrate fabrication and optimization. YG, KZ, TR and AB acknowledges financial support from the Danish National Research Foundation (DNRF122), Villum Fonden (Grant no. 9301) for Intelligent Drug delivery and sensing Using microcontainers and Nanomechanics (IDUN) and BioInnovation Institute Foundation for Therapeutic drug monitoring (Grant no. NNF20SA0063552). KS acknowledges financial support from Danish Cancer Society (grant no R257-A14720) and Danish Childhood Cancer Foundation (Grant no 2019-5934 and 2020-6759).

REFERENCES

(1) Kang, J.-S.; Lee, M.-H. Overview of Therapeutic Drug Monitoring. *Korean J. Intern. Med.* **2009**. https://doi.org/10.3904/kjim.2009.24.1.1.

(2) Soldin, O. P.; Soldin, S. J. Review: Therapeutic Drug Monitoring in Pediatrics. In *Therapeutic Drug Monitoring*; 2002;

Vol. 24, pp 1–8. https://doi.org/10.1097/00007691-200202000-00001.

(3) Paci, A.; Veal, G.; Bardin, C.; Levêque, D.; Widmer, N.; Beijnen, J.; Astier, A.; Chatelut, E. Review of Therapeutic Drug Monitoring of Anticancer Drugs Part 1 - Cytotoxics. *Eur. J. Cancer* **2014**, *50* (12), 2010–2019. https://doi.org/10.1016/j.ejca.2014.04.014.

(4) Schmiegelow, K. Advances in Individual Prediction of Methotrexate Toxicity: A Review. *British Journal of Haematology*. 2009, pp 489–503. https://doi.org/10.1111/j.1365-2141.2009.07765.x.

(5) Howard, S. C.; McCormick, J.; Pui, C.; Buddington, R. K.; Harvey, R. D. Preventing and Managing Toxicities of High-Dose Methotrexate. *Oncologist* **2016**, *21* (12), 1471–1482. https://doi.org/10.1634/theoncologist.2015-0164.

(6) Widemann, B. C.; Adamson, P. C. Understanding and Managing Methotrexate Nephrotoxicity. *Oncologist* **2006**, *11* (6), 694–703. https://doi.org/10.1634/theoncologist.11-6-694.

(7) Donelli, M. G.; D, B. S.; Zucchetti, M.; Chem, D. Pharmacokinetics of. **1995**, *159*, 154–159.

(8) Piard, C.; Bressolle, F.; Fakhoury, M.; Zhang, D.; Yacouben, K.; Rieutord, A.; Jacqz-Aigrain, E. A Limited Sampling Strategy to Estimate Individual Pharmacokinetic Parameters of Methotrexate in Children with Acute Lymphoblastic Leukemia. *Cancer Chemother. Pharmacol.* **2007**, *60* (4), 609–620. https://doi.org/10.1007/s00280-006-0394-3.

(9) Svahn, T.; Mellgren, K.; Harila-Saari, A.; Åsberg, A.; Kanerva, J.; Jónsson, Ó.; Vaitkeviciene, G.; Stamm Mikkelssen, T.; Schmiegelow, K.; Heldrup, J. Delayed Elimination of High-Dose Methotrexate and Use of Carboxypeptidase G2 in Pediatric Patients during Treatment for Acute Lymphoblastic Leukemia. *Pediatr. Blood Cancer* **2017**, *64* (7). https://doi.org/10.1002/pbc.26395.

(10) DeAngelis, L. M.; Tong, W. P.; Lin, S.; Fleisher, M.; Bertino, J. R. Carboxypeptidase G2 Rescue after High-Dose Methotrexate. *J. Clin. Oncol.* **1996**, *14* (7), 2145–2149. https://doi.org/10.1200/JCO.1996.14.7.2145.

(11) Ramsey, L. B.; Balis, F. M.; O'Brien, M. M.; Schmiegelow, K.; Pauley, J. L.; Bleyer, A.; Widemann, B. C.; Askenazi, D.; Bergeron, S.; Shirali, A.; Schwartz, S.; Vinks, A. A.; Heldrup, J. Consensus Guideline for Use of Glucarpidase in Patients with High-Dose Methotrexate Induced Acute Kidney Injury and Delayed Methotrexate Clearance. *Oncologist* **2018**, *23* (1), 52–61. https://doi.org/10.1634/theoncologist.2017-0243.

(12) Trifilio, S.; Ma, S.; Petrich, A. Reduced-Dose Carboxypeptidase-G2 Successfully Lowers Elevated Methotrexate Levels in an Adult with Acute Methotrexate-Induced Renal Failure. *Clin. Adv. Hematol. Oncol.* **2013**, *11* (5), 322–323.

(13) Karami, F.; Ranjbar, S.; Ghasemi, Y.; Negahdaripour, M. Analytical Methodologies for Determination of Methotrexate and Its Metabolites in Pharmaceutical, Biological and Environmental Samples. *J. Pharm. Anal.* **2019**, *9* (6), 373–391. https://doi.org/10.1016/j.jpha.2019.06.001.

(14) Li, Y. D.; Li, Y.; Liang, N. S.; Yang, F.; Kuang, Z. P. A Reversed-Phase High Performance Liquid Chromatography Method for Quantification of Methotrexate in Cancer Patients Serum. *J. Chromatogr. B Anal. Technol. Biomed. Life Sci.* **2015**, *1002*, 107–112. https://doi.org/10.1016/j.jchromb.2015.08.017.

(15) Uchiyama, M.; Matsumoto, T.; Matsumoto, T.; Jimi, S.; Takamatsu, Y.; Tamura, K.; Hara, S. Simple and Sensitive HPLC Method for the Fluorometric Determination of Methotrexate and Its Major Metabolites in Human Plasma by Post-Column Photochemical Reaction. *Biomed. Chromatogr.* **2012**, *26* (1), 76–80. https://doi.org/10.1002/bmc.1628.

(16) Mei, S.; Shi, X.; Du, Y.; Cui, Y.; Zeng, C.; Ren, X.; Yu, K.; Zhao, Z.; Lin, S. Simultaneous Determination of Plasma Methotrexate and 7-Hydroxy Methotrexate by UHPLC–MS/MS in Patients Receiving High-Dose Methotrexate Therapy. *J. Pharm. Biomed. Anal.* **2018**, *158*, 300–306. https://doi.org/10.1016/j.jpba.2018.06.011.

(17) Al-Ghobashy, M. A.; Hassan, S. A.; Abdelaziz, D. H.; Elhosseiny, N. M.; Sabry, N. A.; Attia, A. S.; El-Sayed, M. H. Development and Validation of LC–MS/MS Assay for the Simultaneous Determination of Methotrexate, 6-Mercaptopurine and Its Active Metabolite 6-Thioguanine in Plasma of Children with Acute Lymphoblastic Leukemia: Correlation with Genetic Polymorphism. *J. Chromatogr. B Anal. Technol. Biomed. Life Sci.* **2016**, *1038*, 88–94. https://doi.org/10.1016/j.jchromb.2016.10.035.

(18) Sonemoto, E.; Kono, N.; Ikeda, R.; Wada, M.; Ueki, Y.; Nakashima, K. Practical Determination of Methotrexate in Serum of Rheumatic Patients by LC-MS/MS. *Biomed. Chromatogr.* **2012**, *26* (11), 1297–1300. https://doi.org/10.1002/bmc.2700.

(19) Freudenberger, K.; Hilbig, U.; Gauglitz, G. Recent Advances in Therapeutic Drug Monitoring of Immunosuppressive Drugs. *TrAC - Trends in Analytical Chemistry*. 2016, pp 257–268. https://doi.org/10.1016/j.trac.2015.11.016.

(20) Slørdal, L.; Prytz, P. S.; Pettersen, I.; Aarbakke, J. Methotrexate Measurements in Plasma: Comparison of Enzyme Multiplied Immunoassay Technique, Tdx Fluorescence Polarization Immunoassay, and High Pressure Liquid Chromatography. *Ther. Drug Monit.* **1986**, *8* (3), 368–372. https://doi.org/10.1097/00007691-198609000-00024.

(21) Albertioni, F.; Rask, C.; Eksborg, S.; Poulsen, J. H.; Pettersson, B.; Beck, O.; Schroeder, H.; Peterson, C. Evaluation of Clinical Assays for Measuring High-Dose Methotrexate in Plasma. *Clin. Chem.* **1996**, *42* (1), 39–44. https://doi.org/10.1093/clinchem/42.1.39.

(22) Widemann, B. C.; Balis, F. M.; Murphy, R. F.; Sorensen, J. M.; Montello, M. J.; O'Brien, M.; Adamson, P. C. Carboxypeptidase-G2, Thymidine, and Leucovorin Rescue in Cancer Patients with Methotrexate-Induced Renal Dysfunction. *J. Clin. Oncol.* **1997**, *15* (5), 2125–2134. https://doi.org/10.1200/JCO.1997.15.5.2125.

(23) Montemurro, M.; De Zan, M. M.; Robles, J. C. Optimized High Performance Liquid Chromatography-Ultraviolet Detection Method Using Core-Shell Particles for the Therapeutic Monitoring of Methotrexate. *J. Pharm. Anal.* **2016**, *6* (2), 103–111. https://doi.org/10.1016/j.jpha.2015.12.001.

(24) Sharma, K.; Giri, K.; Dhiman, V.; Dixit, A.; Zainuddin, M.; Mullangi, R. A Validated LC-MS/MS Assay for Simultaneous Quantification of Methotrexate and Tofacitinib in Rat Plasma: Application to a Pharmacokinetic Study. *Biomed. Chromatogr.* **2015**, *29* (5), 722–732. https://doi.org/10.1002/bmc.3348.

(25) Begas, E.; Papandreou, C.; Tsakalof, A.; Daliani, D.; Papatsibas, G.; Asprodini, E. Simple and Reliable HPLC Method for the Monitoring of Methotrexate in Osteosarcoma Patients. *J. Chromatogr. Sci.* **2014**, *52* (7), 590–595. https://doi.org/10.1093/chromsci/bmt081.

(26) Sottani, C.; Turci, R.; Perbellini, L.; Minoia, C. Liquid–liquid Extraction Procedure for Trace Determination of Cyclophosphamide in Human Urine by High-performance Liquid Chromatography Tandem Mass Spectrometry. *Rapid Commun. Mass Spectrom.* **1998**, *12* (16), 1063–1068. https://doi.org/10.1002/(sici)1097-0231(19980831)12:16<1063::aid-rcm287>3.3.co;2-b.

(27) Thappali, S. R. S.; Varanasi, K. V. S.; Veeraraghavan, S.; Vakkalanka, S. K. V. S.; Khagga, M. Simultaneous Determination of Methotrexate, Dasatinib and Its Active Metabolite N-Deshydroxyethyl Dasatinib in Rat Plasma by LC-MS/MS: Method Validation and Application to Pharmacokinetic Study. *Arzneimittel-Forschung/Drug Res.* **2012**, *62* (12), 624–630. https://doi.org/10.1055/s-0032-1327702.

(28) Ates, H. C.; Roberts, J. A.; Lipman, J.; Cass, A. E. G.; Urban, G. A.; Dincer, C. On-Site Therapeutic Drug Monitoring.

Trends Biotechnol. **2020**, *xx* (xx), 1–16. https://doi.org/10.1016/j.tibtech.2020.03.001.

(29) Griss, R.; Schena, A.; Reymond, L.; Patiny, L.; Werner, D.; Tinberg, C. E.; Baker, D.; Johnsson, K. Bioluminescent Sensor Proteins for Point-of-Care Therapeutic Drug Monitoring. *Nat. Chem. Biol.* **2014**, *10* (7), 598–603. https://doi.org/10.1038/nchembio.1554.

(30) Tenaglia, E.; Ferretti, A.; Decosterd, L. A.; Werner, D.; Mercier, T.; Widmer, N.; Buclin, T.; Guiducci, C. Comparison against Current Standards of a DNA Aptamer for the Label-Free Quantification of Tobramycin in Human Sera Employed for Therapeutic Drug Monitoring. *J. Pharm. Biomed. Anal.* **2018**, *159*, 341–347. https://doi.org/10.1016/j.jpba.2018.06.061.

(31) Zhao, S. S.; Bukar, N.; Toulouse, J. L.; Pelechacz, D.; Robitaille, R.; Pelletier, J. N.; Masson, J. F. Miniature Multi-Channel SPR Instrument for Methotrexate Monitoring in Clinical Samples. *Biosens. Bioelectron.* **2015**, *64*, 664–670. https://doi.org/10.1016/j.bios.2014.09.082.

(32) Dauphin-Ducharme, P.; Yang, K.; Arroyo-Currás, N.; Ploense, K. L.; Zhang, Y.; Gerson, J.; Kurnik, M.; Kippin, T. E.; Stojanovic, M. N.; Plaxco, K. W. Electrochemical Aptamer-Based Sensors for Improved Therapeutic Drug Monitoring and High-Precision, Feedback-Controlled Drug Delivery. *ACS Sensors* **2019**, *4* (10), 2832–2837. https://doi.org/10.1021/acssensors.9b01616.

(33) Fahem, D. K.; El Houssini, O. M.; Abd El-Rahman, M. K.; Zaazaa, H. E. A Point of Care Screen Printed Potentiometric Sensor for Therapeutic Monitoring of Vecuronium. *Microchem. J.* **2019**, *147*, 532–537. https://doi.org/10.1016/j.microc.2019.03.065.

(34) Jaworska, A.; Fornasaro, S.; Sergo, V.; Bonifacio, A. Potential of Surface Enhanced Raman Spectroscopy (SERS) in Therapeutic Drug Monitoring (TDM). A Critical Review. *Biosensors* **2016**, *6* (3). https://doi.org/10.3390/bios6030047.

(35) SERSTECH https://serstech.com/our-offer/serstech-arx/ (accessed Jan 21, 2021).

(36) TRU SCAN https://www.thermofisher.com/order/catalog/product/TRUSCANRM?gclid=CjwKCAiA6aSABhApEiwA6Cbm_-zUIfT5yX2Xakd7FBNHa5foHxOahTVREod9ls9KriW_reSvlPfJvxoCXEAQAvD_BwE&cid=cad_fsi_pharma_brand_adwords&ef_id=CjwKCAiA6aSABhApEiwA6Cbm_-zUIfT5yX2Xakd7FBNHa5foHxOahTVRE (accessed Jan 21, 2021).

(37) Mochizuki, K.; Smith, N. I.; Fujita, K. Raman Spectroscopy | Raman Microscopy. In *Encyclopedia of Analytical Science*; 2019; pp 58–67. https://doi.org/10.1016/B978-0-12-409547-2.14016-8.

(38) Fan, F.; Feng, Z.; Li, C. Raman and UV-Raman Spectroscopies. In *Characterization of Solid Materials and Heterogeneous Catalysts: From Structure to Surface Reactivity, Volume 1&2*; 2012; Vol. 1, pp 49–87. https://doi.org/10.1002/9783527645329.ch2.

(39) Graham, D.; Van Duyne, R.; Ren, B. Surface-Enhanced Raman Scattering. *Analyst*. 2016, p 4995. https://doi.org/10.1039/c6an90064j.

(40) Le Ru, E. C.; Etchegoin, P. G. *Principles of Surface-Enhanced Raman Spectroscopy*; 2009. https://doi.org/10.1016/B978-0-444-52779-0.X0001-3.

(41) Langer, J. et al. Present and Future of Surface-Enhanced Raman Scattering. *ACS Nano*. 2020, pp 28–117. https://doi.org/10.1021/acsnano.9b04224.

(42) Durucan, O.; Rindzevicius, T.; Schmidt, M. S.; Matteucci, M.; Boisen, A. Nanopillar Filters for Surface-Enhanced Raman Spectroscopy. *ACS Sensors* **2017**, *2* (10), 1400–1404. https://doi.org/10.1021/acssensors.7b00499.

(43) Viehrig, M.; Rajendran, S. T.; Sanger, K.; Schmidt, M. S.; Alstrøm, T. S.; Rindzevicius, T.; Zór, K.; Boisen, A. Quantitative SERS Assay on a Single Chip Enabled by Electrochemically Assisted Regeneration: A Method for Detection of Melamine in Milk. *Anal. Chem.* **2020**, *92* (6), 4317–4325. https://doi.org/10.1021/acs.analchem.9b05060.

(44) Rostami, S.; Zór, K.; Zhai, D. S.; Viehrig, M.; Morelli, L.; Mehdinia, A.; Smedsgaard, J.; Rindzevicius, T.; Boisen, A. High-Throughput Label-Free Detection of Ochratoxin A in Wine Using Supported Liquid Membrane Extraction and Ag-Capped Silicon Nanopillar SERS Substrates. *Food Control* **2020**, *113*. https://doi.org/10.1016/j.foodcont.2020.107183.

(45) Morelli, L.; Zór, K.; Jendresen, C. B.; Rindzevicius, T.; Schmidt, M. S.; Nielsen, A. T.; Boisen, A. Surface Enhanced Raman Scattering for Quantification of P-Coumaric Acid Produced by Escherichia Coli. *Anal. Chem.* **2017**, *89* (7), 3981–3987. https://doi.org/10.1021/acs.analchem.6b04428.

(46) Morelli, L.; Andreasen, S. Z.; Jendresen, C. B.; Nielsen, A. T.; Emnéus, J.; Zór, K.; Boisen, A. Quantification of a Bacterial Secondary Metabolite by SERS Combined with SLM Extraction for Bioprocess Monitoring. *Analyst* **2017**, *142* (23), 4553–4559. https://doi.org/10.1039/c7an01393k.

(47) Hakonen, A.; Wu, K.; Stenbæk Schmidt, M.; Andersson, P. O.; Boisen, A.; Rindzevicius, T. Detecting Forensic Substances Using Commercially Available SERS Substrates and Handheld Raman Spectrometers. *Talanta* **2018**. https://doi.org/10.1016/j.talanta.2018.07.009.

(48) Yang, L.; Chen, Y.; Li, H.; Luo, L.; Zhao, Y.; Zhang, H.; Tian, Y. Application of Silver Nanoparticles Decorated with β-Cyclodextrin in Determination of 6-Mercaptopurine by Surface-Enhanced Raman Spectroscopy. *Anal. Methods* **2015**, *7* (16), 6520–6527. https://doi.org/10.1039/c5ay01212k.

(49) Wu, H. Y.; Cunningham, B. T. Point-of-Care Detection and Real-Time Monitoring of Intravenously Delivered Drugs via Tubing with an Integrated SERS Sensor. *Nanoscale* **2014**, *6* (10), 5162–5171. https://doi.org/10.1039/c4nr00027g.

(50) N.E., M.; I.Y., G.; A.V., M. Sample Pretreatment and SERS-Based Detection of Ceftriaxone in Urine. *Anal. Bioanal. Chem.* **2018**, *410* (8), 2221–2227. https://doi.org/10.1007/s00216-018-0888-y LK - http://rug.on.worldcat.org/atoztitles/link/?sid=EMBASE&issn=16182650&id=doi:10.1007%2Fs00216-018-0888-y&atitle=Sample+pretreatment+and+SERS-based+detection+of+ceftriaxone+in+urine&stitle=Anal+Bioanal+Chem&title=Analytical+and+bioanalytical+chemistry&volume=410&issue=8&spage=2221&epage=2227&aulast=Markina&aufirst=Natalia+E.&auinit=N.E.&aufull=Markina+N.E.&coden=&isbn=&pages=2221-2227&date=2018&auinit1=N&auinitm=E.

(51) Fornasaro, S.; Marta, S. D.; Rabusin, M.; Bonifacio, A.; Sergo, V. Toward SERS-Based Point-of-Care Approaches for Therapeutic Drug Monitoring: The Case of Methotrexate. *Faraday Discuss.* **2016**, *187*, 485–499. https://doi.org/10.1039/c5fd00173k.

(52) McLaughlin, C.; MacMillan, D.; McCardle, C.; Smith, W. E. Quantitative Analysis of Mitoxantrone by Surface-Enhanced Resonance Raman Scattering. *Anal. Chem.* **2002**, *74* (13), 3160–3167. https://doi.org/10.1021/ac010067k.

(53) Morelli, L.; Serioli, L.; Centorbi, F. A.; Jendresen, C. B.; Matteucci, M.; Ilchenko, O.; Demarchi, D.; Nielsen, A. T.; Zór, K.; Boisen, A. Injection Molded Lab-on-a-Disc Platform for Screening of Genetically Modified: E. Coli Using Liquid-Liquid Extraction and Surface Enhanced Raman Scattering. *Lab Chip* **2018**, *18* (6), 869–877. https://doi.org/10.1039/c7lc01217a.

(54) Jiang, X.; Zhang, J.; Xu, L.; Wang, W.; Du, J.; Qu, M.; Han, X.; Yang, L.; Zhao, B. Ultrasensitive SERS Detection of Antitumor Drug Methotrexate Based on Modified Ag Substrate. *Spectrochim. Acta - Part A Mol. Biomol. Spectrosc.* **2020**, *240*. https://doi.org/10.1016/j.saa.2020.118589.

(55) Hidi, I. J.; Mühlig, A.; Jahn, M.; Liebold, F.; Cialla, D.; Weber, K.; Popp, J. LOC-SERS: Towards Point-of-Care Diagnostic of Methotrexate. *Anal. Methods* **2014**, *6* (12), 3943–3947. https://doi.org/10.1039/c3ay42240b.

(56) Chen, M.; Tang, J.; Luo, W.; Zhang, Z.; Zhu, Y.; Wang, R.; Yang, H.; Chen, X. Core-Shell-Satellite Microspheres-Modified Glass Capillary for Microsampling and Ultrasensitive SERS Spectroscopic Detection of Methotrexate in Serum. *Sensors Actuators, B Chem.* **2018**, *275*, 267–276. https://doi.org/10.1016/j.snb.2018.08.048.

(57) Parachalil, D. R.; Commerford, D.; Bonnier, F.; Chourpa, I.; McIntyre, J.; Byrne, H. J. Raman Spectroscopy as a Potential Tool for Label Free Therapeutic Drug Monitoring in Human Serum: The Case of Busulfan and Methotrexate. *Analyst* **2019**, *144* (17), 5207–5214. https://doi.org/10.1039/c9an00801b.

(58) Markina, N. E.; Zakharevich, A. M.; Markin, A. V. Determination of Methotrexate in Spiked Human Urine Using SERS-Active Sorbent. *Anal. Bioanal. Chem.* **2020**, *412* (28), 7757–7766. https://doi.org/10.1007/s00216-020-02932-x.

(59) Subaihi, A.; Trivedi, D. K.; Hollywood, K. A.; Bluett, J.; Xu, Y.; Muhamadali, H.; Ellis, D. I.; Goodacre, R. Quantitative Online Liquid Chromatography-Surface-Enhanced Raman Scattering (LC-SERS) of Methotrexate and Its Major Metabolites. *Anal. Chem.* **2017**, *89* (12), 6702–6709. https://doi.org/10.1021/acs.analchem.7b00916.

(60) Durucan, O.; Wu, K.; Viehrig, M.; Rindzevicius, T.; Boisen, A. Nanopillar-Assisted SERS Chromatography. *ACS Sensors* **2018**, *3* (12), 2592–2598. https://doi.org/10.1021/acssensors.8b00887.

(61) Schmidt, M. S.; Hübner, J.; Boisen, A. Large Area Fabrication of Leaning Silicon Nanopillars for Surface Enhanced Raman Spectroscopy. *Adv. Mater.* **2012**, *24* (10). https://doi.org/10.1002/adma.201103496.

(62) Newman, M. E. J. Power Laws, Pareto Distributions and Zipf's Law. *Contemp. Phys.* **2005**, *46* (5), 323–351. https://doi.org/10.1080/00107510500052444.

(63) Yang, J.; Palla, M.; Bosco, F. G.; Rindzevicius, T.; Alstrøm, T. S.; Schmidt, M. S.; Boisen, A.; Ju, J.; Lin, Q. Surface-Enhanced Raman Spectroscopy Based Quantitative Bioassay on Aptamer-Functionalized Nanopillars Using Large-Area Raman Mapping. *ACS Nano* **2013**, *7* (6), 5350–5359. https://doi.org/10.1021/nn401199k.

(64) Hakonen, A.; Svedendahl, M.; Ogier, R.; Yang, Z. J.; Lodewijks, K.; Verre, R.; Shegai, T.; Andersson, P. O.; Käll, M. Dimer-on-Mirror SERS Substrates with Attogram Sensitivity Fabricated by Colloidal Lithography. *Nanoscale* **2015**, *7* (21), 9405–9410. https://doi.org/10.1039/c5nr01654a.

(65) Ayyappan, S.; Sundaraganesan, N.; Aroulmoji, V.; Murano, E.; Sebastian, S. Molecular Structure, Vibrational Spectra and DFT Molecular Orbital Calculations (TD-DFT and NMR) of the Antiproliferative Drug Methotrexate. *Spectrochim. Acta - Part A Mol. Biomol. Spectrosc.* **2010**, *77* (1), 264–275. https://doi.org/10.1016/j.saa.2010.05.021.

(66) Skärby, T. V. C.; Anderson, H.; Heldrup, J.; Kanerva, J. A.; Seidel, H.; Schmiegelow, K. High Leucovorin Doses during High-Dose Methotrexate Treatment May Reduce the Cure Rate in Childhood Acute Lymphoblastic Leukemia. *Leukemia* **2006**, *20* (11), 1955–1962. https://doi.org/10.1038/sj.leu.2404404.

(67) Flombaum, C. D.; Meyers, P. A. High-Dose Leucovorin as Sole Therapy for Methotrexate Toxicity. *J. Clin. Oncol.* **1999**, *17* (5), 1589–1594. https://doi.org/10.1200/jco.1999.17.5.1589.

(68) Bonifacio, A.; Dalla Marta, S.; Spizzo, R.; Cervo, S.; Steffan, A.; Colombatti, A.; Sergo, V. Surface-Enhanced Raman Spectroscopy of Blood Plasma and Serum Using Ag and Au Nanoparticles: A Systematic Study. *Anal. Bioanal. Chem.* **2014**, *406* (9–10), 2355–2365. https://doi.org/10.1007/s00216-014-7622-1.